Controllable Growth of Cobalt Oxide Nanoparticles on Reduced Graphene Oxide and its Application for Highly Sensitive Glucose Sensor

Yaolin Zheng, Ping Li, Hongbo Li, Shouhui Chen[*]

Key Laboratory of Functional Small Organic Molecule, Ministry of Education, College of Chemistry and Chemical Engineering, Jiangxi Normal University, Nanchang 330022, China.
[*]E-mail: shchengroup@126.com

A nonenzymatic glucose sensor was developed by using the reduced graphene oxide (rGO) and Co_3O_4 nanocomposites as the sensing material. The hybrid was prepared in a one-pot reaction process by hydrothermal method. The effects of time and temperature in the hydrothermal treatment on the Co_3O_4-rGO nanocomposites were explored. Co_3O_4 with size of 5-10 nm was successfully synthesized on the surface of rGO at 150 °C for 3 h. These Co_3O_4-rGO nanocomposites exhibited superior electrochemical activity towards oxidation of glucose. The catalytic current density is linear to the glucose concentration in the range of 0.0005 mM to 1.277 mM with a sensitivity of 1366 $\mu A\ cm^{-2}\ mM^{-1}$ and a detection limit of 0.18 μM. The high sensitivity, low detection limit and good selectivity indicate that the newly developed sensor based on the Co_3O_4-rGO nanocomposites is a promising sensor for practical application.

1. INTRODUCTION

With the development of society and the improvement of human's physical life, the diabetes mellitus has become one of the major afflictions that seriously threatens human health worldwide [1,2]. Therefore, monitoring glucose concentration in foods and pharmaceuticals is very important in practical applications [3,4]. Enzymatic glucose sensors have been developed for continuous glucose detection due to their excellent selectivity, high sensitivity and low detection limit [1,5]. However, enzyme-based glucose biosensors was usually suffer from many disadvantages such as poor stability originated from the pH, temperature, humidity and oxygen levels of enzymes [6]. Hence, nonenzymatic glucose sensors have raised particular interest owing to its advantages including stability, simplicity, and free of oxygen limitation.

Noble metal nanoparticles (NPs) including Pt [7] and Au [8] have been used to modify the electrodes for glucose detection with wide linear range and low working potential. But the expensive price of noble metals (Pt and Au) limits its widespread application. Hence, non-noble metal or non-noble metal oxide, such as Cu [9], CuO [10], Ni [11], NiO [12] etc, have attracted increasing attention due to its low cost and high sensitivity for glucose. The practical application of those materials was limited by its poor selectivity [13]. Cobalt and cobat oxide NPs, which has been widely used in nonenzymatic amino acid sensors but rarely reported for glucose detection, may be the suitable mimetic enzyme for glucose detection because of its excellent anti-interference property, high surface area and good electrochemical stability as well as low cost for practical applications [14,15]. However, the pure Co_3O_4 NPs could form severe particle aggregation structures after they are assembled on an electrode, which will reduce their specific surface and hinder the mass transfer [16]. Therefore, an effective way to enhance the electrochemical performance is to combine Co_3O_4 with carbon materials.

Reduced graphene oxide (rGO), the thinnest two-dimensional carbon material, may be the most suitable substrate to support metal nanomaterials because of its high electrical conductivity and specific surface properties (2630 m^2 g^{-1}) [17,18]. Up to now, many works have been reported for synthesizing rGO by the strong reducing agents such as $NaBH_4$ or hydrazine. Besides, most of these preparation methods were complicated with multistep reaction process or strict reaction condition, and the application of strong reducing agents would leave lots of chemical residues, which not only bring environmental pollution but also cause the waste of resources. Over the past decade, many sensors have been developed for the detection of glucose based on cobalt or cobalt oxide with low detection limit. But most of them were limited to its poor sensitivity, narrow linear range and long response time [19,20].

In this work, a simple and environment friendly strategy was employed to prepare the Co_3O_4-rGO in ethanol solution by hydrothermal method. In this method, ethanol not only serves as the solvents for hydrothermal reaction, but also acts as a green reductant of graphene oxide (GO), which successfully reduces the GO into high conductivity rGO. As a result, Co_3O_4 NPs with size of 5-10 nm were evenly distributed on the surface of rGO, at the same time GO could be partly reduced by ethanol. Compared with other method, our method for the preparation of Co_3O_4-rGO nanocomposites has many advantages such as low cost, non-toxic and simplicity in process. The Co_3O_4-rGO nanocomposites were successfully modified on glassy carbon electrode (GCE) and used as nonenzymatic glucose sensors. The as-fabricated electrode exhibits large electrochemical active surface area, high utilization efficiency of active materials and superior mass transport property towards the oxidation of glucose. The catalytic current density is linear to the glucose concentration in the range of 0.0005 mM to 1.277 mM with a high sensitivity of 1366 μA cm^{-2} mM^{-1} and a low detection limit of 0.18 μM. The rapid response of as-prepared sensor makes it possible to be applied in the fast detection of glucose.

2. EXPERIMENTAL PART

2.1 Chemicals and reagents

Graphite powder, ethanol, glucose, L-ascorbic acid (AA), uric acid (UA), dopamine (DA), D-galactose, and fructose were purchased from Sinopharm Chemical Reagent Co., Ltd (Shanghai,

China). $Co(CH_3COO)_2 \cdot 4H_2O$ was obtained from Sigma-Aldrich. $NH_3 \cdot H_2O$ (25-28 wt%) was purchased from Tianjin Yongda Chemical Reagent Factory (Tianjin, China). NaOH were purchased from Tianjin Fuchen Chemical Reagent Factory (Tianjin, China). Other reagents were purchased from Beijing Chemical Reagent Factory (Beijing, China). All reagents were of analytical grade and used without further purification. All solutions were prepared with ultra-pure water, purified by a Millipore-Q system (18.2 MΩ cm).

2.2 Instrumentations

Scanning electron microscopy (SEM) images and energy dispersive spectrometer (EDS) were obtained by using a HITACHI SU-8020 scanning electron microscope equipped with an energy dispersive X-ray analyzer at an accelerating voltage of 20 kV. Fourier transform infrared spectroscopy (FT-IR) spectroscopy was recorded on a Perkin–Elmer Spectrome 100 spectrometer (Perkin-Elmer Company, USA) by using KBr pellets. Raman spectra were acquired with a Horiba Jobin Yvon LabRam HR Raman spectrometer. X-ray powder diffraction (XRD) data were collected on a D/Max 2500 V/PC X-ray powder diffractometer by using Cu Kα radiation (λ= 1.54056 Å, 40 kV, 200 mA). All electrochemical experiments were performed on a CHI760d electrochemical workstation (CH Instruments, Shanghai, China) using a conventional three-electrode system with a platinum wire as the auxiliary electrode, a modified GCE as the working electrode, and a saturated calomel electrode (SCE) as the reference electrode. The cyclic voltammetric experiments were performed in a quiescent solution. The amperometric were carried out in a beaker with continuous stirring using a magnetic stirrer.

2.3 Synthesis of GO and Co_3O_4-rGO

The GO was synthesized according to Hummers' method [21]. The Co_3O_4-rGO nanocomposites were prepared as follows: 72 mg GO and 2.0 mL ultra-pure water was added into 80 mL EtOH, and then ultrasound dispersed for 30 min. Next, 3.0 mL of 0.5 M $Co(CH_3COO)_2$ was added into the above solution under stirring and then 2 mL $NH_3 \cdot H_2O$ (25-28 wt%) was added. After that, the mixture was stirred for 1 h at 80 ºC. Lastly, the mixed product (about 70 mL) was transferred into a Teflon-lined stainless steel autoclave with a volume of 100 mL, and a thermal treatment was performed in an oven at 150 °C for 3 h. The product was centrifuged and washed with ethanol and water to obtain the Co_3O_4-rGO nanocomposites. For comparison, rGO was made through the same procedure as Co_3O_4-rGO nanocomposites without adding any Co salt in the second step. Pure Co_3O_4 NPs were obtained through the same steps as making Co_3O_4-rGO nanocomposites without adding any GO in the first step.

2.4 Electrode modification

GCE was first polished with 1.0 μm and 0.3 μm alumina powders. After rinsing thoroughly with deionized water, it was sonicated in ethanol and deionized water to remove any alumina residues,

then, the GCE was allowed to dry in a stream of nitrogen. Then 6 µL of the ink-like suspension of corresponding materials (2 mg/mL) was cast on the surface of clean GCE and dried in an inverted beaker at room temperature. Finally, a drop of Nafion aqueous solution (5 µL, 0.05 wt%) was coated on the modified electrode and dried in air.

3. RESULTS AND DISCUSSION

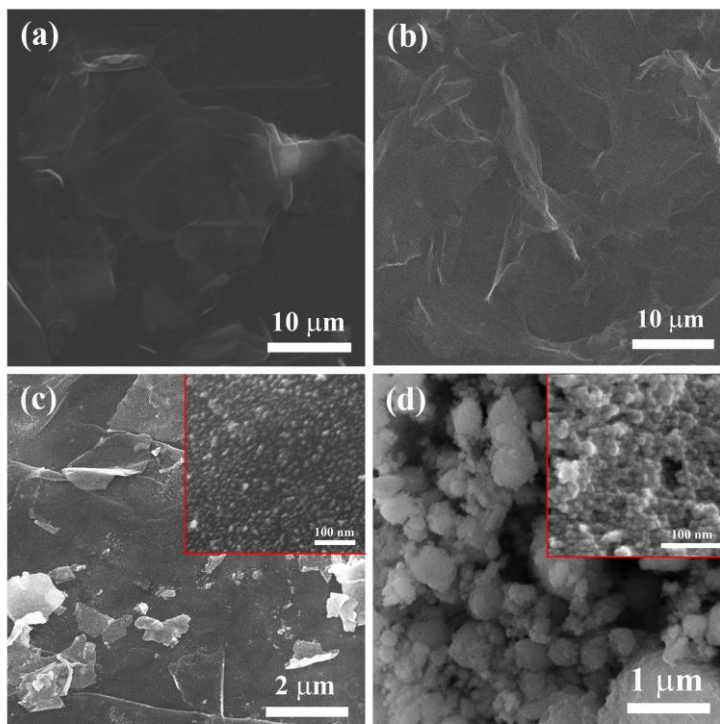*3.1 Characteristics of the Co_3O_4-rGO nanocomposites*

Figure 1. SEM images of the (a) GO, (b) rGO, (c) Co_3O_4-rGO and (d) Co_3O_4.

The morphologies of as-synthesized Co_3O_4-rGO were firstly characterized by SEM. As shown in Figure 1a, a typical SEM image of the GO was obtained with smooth and homogeneous nanosheets. Figure 1b showed the SEM image of the rGO consisting of curled and crumpled solid sheets, which was prepared by ethanol hydrothermal reduction. Figure 1c revealed the SEM images of Co_3O_4-rGO. It clearly demonstrates that the Co_3O_4 NPs with size of 5-10 nm were evenly distributed on the surface of rGO. For comparison, pure Co_3O_4 NPs were synthesized through the same steps as making Co_3O_4-rGO nanocomposites without adding any GO. As shown in Figure 1d, NPs with size of 5-10 nm were also be found in the pure Co_3O_4, but the Co_3O_4 NPs severely aggregated and formed close-packed structures. It indicates clearly that the presence of rGO played a key role in the growth of Co_3O_4 NPs. The high conductivity rGO provided a large specific surface area with more binding-sites to greatly increase the dispersion of Co_3O_4 NPs [22].

EDS was used to study the components of those nanocomposites (Figure 2a). The inserted table in Figure 2a demonstrated that the ratio of C/O was greatly increased after solvothermal reduction, suggesting that GO was successfully reduced into rGO by ethanol. FT-IR spectra of GO, rGO and Co_3O_4-rGO nanocomposites are shown in Figure 2b. The curve of GO shows a stretching vibration of C=O at 1730 cm^{-1}, –OH at 3419 cm^{-1} and C–OH at 1395 cm^{-1}. The spectrum also shows peak at 1064 cm^{-1}originated from the C–O stretching vibrations of alkoxy.
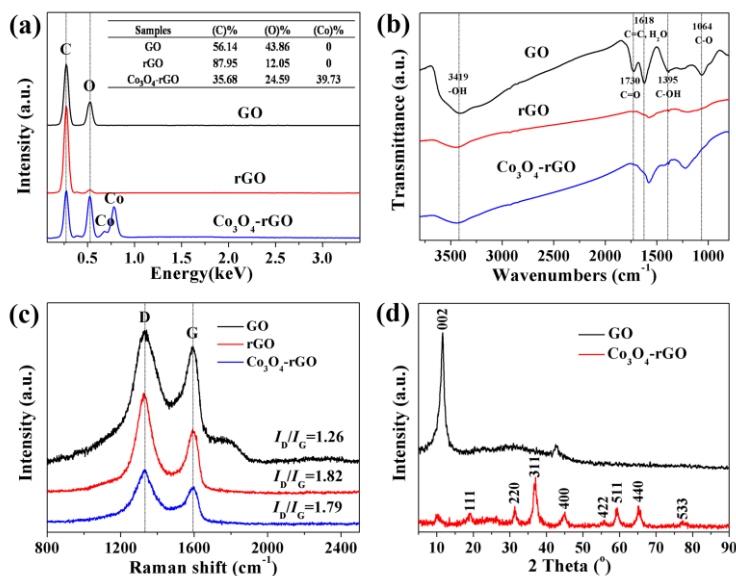

Figure 2. (a-c) EDS analysis (a), FT-IR (b) and Raman spectra (c) of GO, rGO and Co_3O_4-rGO. (d) XRD pattern of the GO and Co_3O_4-rGO.

The peak at 1618 cm^{-1} is assigned to the vibrations of the adsorbed water molecules and the contributions from the vibration of aromatic C=C [23,24]. For rGO and Co_3O_4-rGO nanocomposites, the bands associated with oxygen-containing functional groups significantly decrease and some of them even disappear. These results further validate an effective removal of the oxygen-containing groups in GO by ethanol. As shown in the Raman spectra (Figure 2c), two prominent peaks of D and G bands locate at about 1332 and 1594 cm^{-1}, respectively. After the hydrothermal treatment, the integrated intensity ratio of the D and G bands (I_D/I_G) was increased from 1.26 (GO) to 1.82 (rGO) or 1.79 (Co_3O_4-rGO). These results indicate that the GO sheet is deoxygenated by the hydrothermal reduction process [25]. The crystal structures of the GO and Co_3O_4-rGO nanocomposites were characterized by XRD as shown in Figure 2d. The XRD pattern of GO exhibited a diffraction peak centered at 11.6º, corresponding to the C (002) interlayer spacing of 0.78 nm [26,27]. The characteristic diffraction peaks at 18.9º, 31.3º, 36.8º, 44.8º, 55.7º, 59.4º, 65.2º and 77.3º were observed for Co_3O_4-rGO nanocomposites, corresponding to the (111), (220), (311), (400), (422), (511), (440) and (533) crystalline planes of Co_3O_4 (JCPDS No. 42-1467), respectively [16,28].

The effects of time (Figure 3a-c) and temperature (Figure 3d-f) in the hydrothermal treatment on the Co_3O_4-rGO nanocomposites have been explored in detail. As shown in Figure 3a (150 ^{o}C for 1

h), only a few Co_3O_4 NPs were formed on the rGO surface. As the thermal treatment time was increased to 3 h (Figure 3b), the quantity of Co_3O_4 NPs increased comparing to 1 h and evenly distributed on the surface of rGO. When further prolonging the thermal treatment time (5 h, Figure 3c), the Co_3O_4 NPs began to aggregate and overlap each other to form bigger nano-cluster.The findings suggest that the thermal treatment time plays a key role in the evolution of Co_3O_4 NPs. The size and the quantity of Co_3O_4 can be controlled by adjusting the thermal treatment time during the hydrothermal. Temperature was another key factor for hydrothermal reaction. After thermal treatment at 120 ^{o}C for 3 h (Figure 3d), the surface of rGO was smooth and it is hard to find Co_3O_4 NPs in the high-magnification image (Inset of Figure 3d). As the temperature was increased to 180 ^{o}C (Figure 3e), a large amount of Co_3O_4 NPs was found in the surface of rGO with an average size about 500 nm, which could be caused by the aggregation of small size Co_3O_4 NPs. When the temperature was further increased to 210 ^{o}C (Figure 3f), the Co_3O_4 NPs became big ones with a size about 1-2 μm. Thus, temperature is the critical factor of the evolution of Co_3O_4 NPs morphology. As we all know, smaller size and uniformly scattered NPs allows rapid transportation of the electrolytes and exhibits high specific surface area [29]. Therefore, Co_3O_4-rGO nanocomposites obtained at 150 ^{o}C for 3 h could be promising materials for glucose sensors.
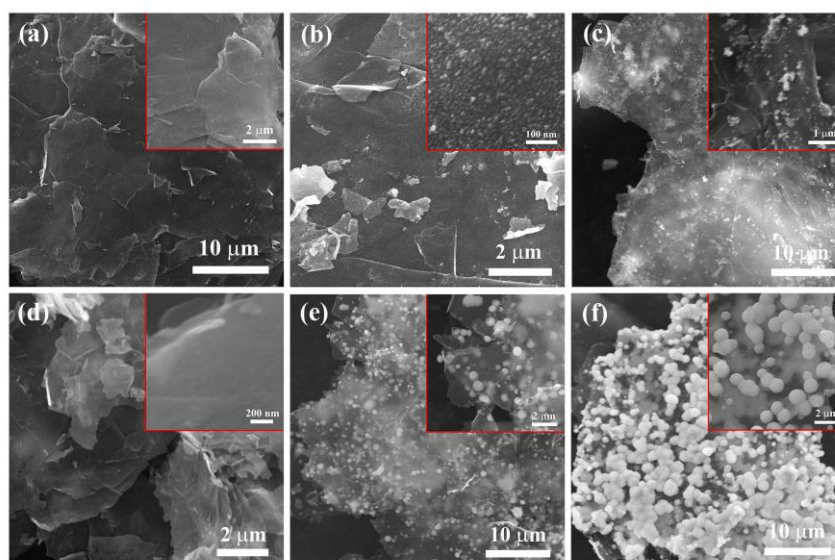

Figure 3. SEM images of the Co_3O_4-rGO nanocomposites obtained at different thermal treatment conditions: (a) 150 ^{o}C-1 hour, (b) 150 ^{o}C-3 hours, (c) 150 ^{o}C-5 hours, (d) 120 ^{o}C-3 hours, (e) 180 ^{o}C-3 hours and (f) 210 ^{o}C-3 hours.

3.2 Electrocatalytic oxidation of glucose at Co_3O_4-rGO/GCE

Figure 4a-c showed the CVs of various modified electrodes in 0.1 M NaOH in the presence (Dotted lines) and absence (Solid lines) of 0.5 mM glucose. In the presence of 0.5 mM glucose, the oxidation peak current density at about 0.55 V obviously increased at the Co_3O_4-rGO/GCE as compared with that in absence of glucose (Figure 4a). Compared with the Co_3O_4/GCE, the Co_3O_4-

rGO/GCE exhibited outstanding electrochemical performance with higher catalytic activity and lower electrocatalytic potential for glucose oxidation. The increase of the electrochemical performance was mainly attributed to the presence of rGO. On the one hand, rGO provided a large surface area to increase the quantity of Co_3O_4 NPs and reduce the dimension of the Co_3O_4 NPs [22]. The large surface-to-volume ratio of the Co_3O_4-rGO nanocomposites produced a large total surface area that provided more chance to contact with glucose. On the other hand, the introducing of rGO enhances conductivity of Co_3O_4-rGO nanocomposites, which was beneficial to higher sensitivity and more negative potentials for glucose oxidation comparing with pure Co_3O_4 [30]. The formation of Co_3O_4-rGO nanocomposites at different time and temperature were also characterized by CVs in 0.1 M NaOH as shown in Figure 4b and 4c. Figure 4d showed the plot of catalytic peak current density (Vertical) and catalytic peak potential (Horizontal) of different electrodes. Comparing with other electrodes (Figure 4d), the Co_3O_4-rGO nanocomposites obtained at 150 °C for 3 h exhibited superior electrochemical performance with higher catalytic current density for glucose. This result might be ascribed to the uniformly scattered small size Co_3O_4 NPs on the surface of rGO, which would be benefit to quickly electron transfer and easy access for glucose to the electrode surfaces, and greatly enhance electrocatalytic performance [31].
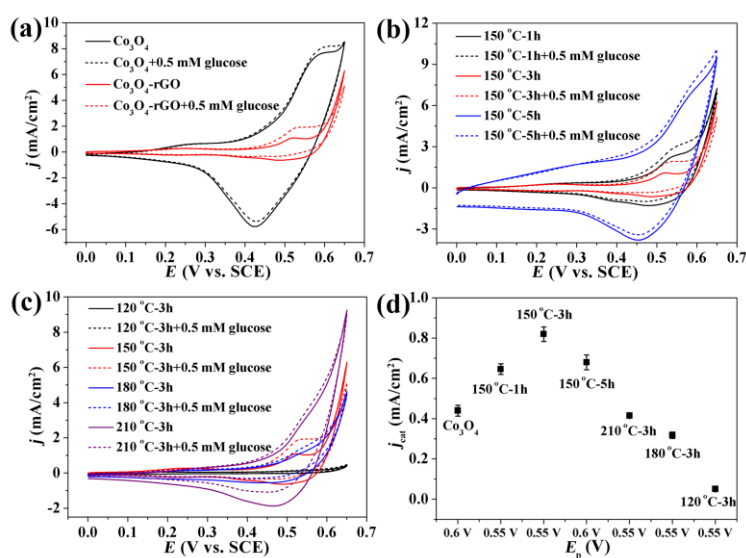

Figure 4. (a-c) CVs of different electrodes in 0.1 M NaOH in absence (Solid lines) and presence of 0.5 mM glucose (Dotted lines) at 50 mV/s: (a) Co_3O_4/GCE and Co_3O_4-rGO/GCE, (b) Co_3O_4-rGO nanocomposites obtained at different thermal treatment time and (c) Co_3O_4-rGO nanocomposites obtained at different thermal treatment temperature. (d) The plot of catalytic peak current density versus the different electrodes.

The electrochemical behaviors of Co_3O_4-rGO/GCE were investigated by CVs at different scan rates in 0.1 M NaOH solution as shown in Figure 5a. Obviously, the peak current was enhanced with the increasing of scan rate. The peak current is proportional to the scan rate as shown by the inset in Figure 5a, indicating that the electron transfer reaction involved a surface-controlled process. The

possible mechanism involving the direct electrochemical process could be described with the following equations [13,15]:
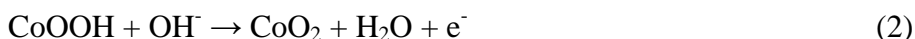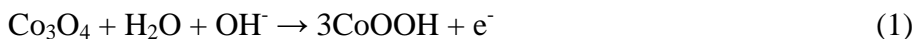
$$Co_3O_4 + H_2O + OH^- \rightarrow 3CoOOH + e^- \qquad (1)$$

$$CoOOH + OH^- \rightarrow CoO_2 + H_2O + e^- \qquad (2)$$

Figure 5b showed the chronoamperometry response for Co_3O_4-rGO/GCE in the absence (curve a) and presence (curve b-e: 0.5-2.0 mM) of glucose. The applied potential steps were 550 mV and 260 mV, respectively. Beginning the applied potential was 550 mV, a large anodic current density occurred because the glucose began to be oxidized. Then as the glucose near electrode surface was oxidized into gluconolactone, the catalytic current density decreased gradually. Finally, a stable concentration difference of glucose between electrode surface and bulk solution was obtained and the catalytic current density was maintained as shown by the curves (a-e) in Figure 5b. The time when the catalytic current density decreased to stable value depends on the catalytic rate constants (K_{cat}) and accordingly the chronoamperograms could be used to calculate the K_{cat} [22]. The relationship between the net current density and the minus square roots of time was shown in inset 1 (Figure 5b), and it revealed a linear dependency. It demonstrated that the electrocatalytic oxidation of glucose was a diffusion-controlled process. The diffusion coefficient (D) of glucose could be estimated according to Cottrell equation [32]:

$$j = \frac{I}{A} = nFD^{1/2}C\pi^{-1/2}t^{-1/2} \qquad (3)$$

where j is the current density, I is the current, A is the electrode surface geometrical area, n is the electron transfer number, F is the Faraday constant (F = 96493 C mol^{-1}), C is the bulk concentration and t is the elapsed time. The mean value of the diffusion coefficient of glucose was found to be 1.935×10^{-3} cm^2 s^{-1} by using the slope of the line in inset 1 (Figure 5b), which was larger than reported value elsewhere [33,34]. Chronoamperometry could also be used for the evaluation of the K_{cat} with the help of the following equation [35]:

$$\frac{j_{cat}}{j_d} = \pi^{1/2}\left(K_{cat}Ct\right)^{1/2} \qquad (4)$$

where j_{cat} and j_d are the catalytic current density and the diffusion-controlled current density, respectively. From the slope of the j_{cat}/j_d vs. $t^{1/2}$ plot, as shown in inset 2 (Figure 5b), the mean value of K_{cat} for glucose was obtained as 1.56×10^6 cm^3 mol^{-1} s^{-1}. The K_{cat} for glucose also was larger than previously reported values [33,36]. The current density for $t > 30$ s were quickly decreased to 0 when potential were stepped down to 260 mV, indicating that the process was inrevisable and accordingly the gluconolactone could not be reduced into glucose by the CoOOH [36].

According to the above results and previous conclusion, the possible redox mechanism can be assumed as shown in Figure 6. In NaOH solution, the Co_3O_4 were firstly oxidized to CoOOH as equation (1), and then the CoOOH were further oxidized into CoO_2, at last the glucose was oxidized by CoO_2, which resulted in the regeneration CoOOH [13,15,19].
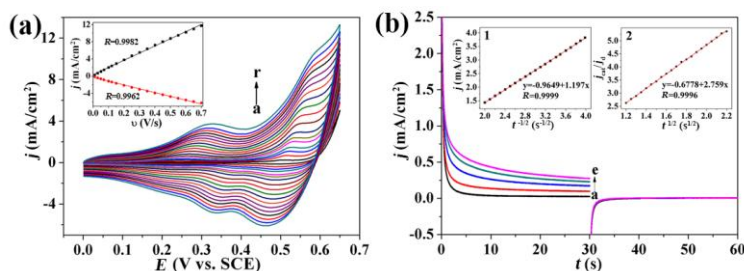
Figure 5. (a) CVs of Co_3O_4-rGO/GCE in 0.1 M NaOH solution at different scan rates: 10 (a), 30 (b), 50 (c), 70 (d), 100 (e), 120 (f), 150 (g), 200 (h), 250 (i), 300 (j), 350 (k), 400 (l), 450 (m), 500 (n), 550 (o), 600 (p), 650 (q) and 700 (r) mV s^{-1}. Inset: Plot of peak current density versus the square root of scan rates. (b) Chronoamperograms of Co_3O_4-rGO/GCE in 0.1 M NaOH solution with different concentrations of glucose: 0 mM (a), 0.5 mM (b), 1 mM (c), 1.5 mM (d) and 2 mM (e). Potential steps were 550 mV and 260 mV, respectively. Inset 1: dependency of transient current density on $t^{-1/2}$. Inset 2: dependency of j_{cat}/j_d on $t^{1/2}$ derived from the data of chronoamperograms of curve a and c in panel (b).
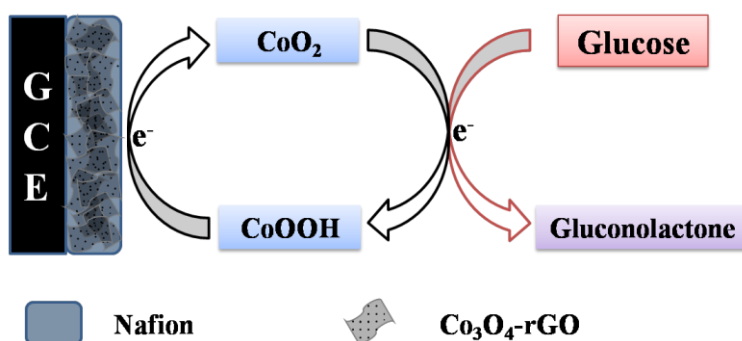

Figure 6. Schematic illustration of glucose electrocatalytic reaction mechanism.

3.3 Amperometric response of the Co_3O_4-rGO/GCE towards glucose

Amperometric measurements were carried out at 0.55 V at the Co_3O_4-rGO/GCE by successive injection of glucose (curve 1 in Figure 7a) into a stirring 0.1 M NaOH. The oxidation current density reached a maximum steady-state value and achieved 95% of the steady-state current density within 2 s. The curve 1 in Figure 7b showed the calibration curve of the sensor. The linear range of the glucose detection was from 0.0005 mM to 1.277 mM ($R=0.9956$) with a slope of 1366 µA cm^{-2} mM^{-1}, and a detection limit of 0.18 µM ($S/N=3$). For comparison, the amperometric response of the Co_3O_4/GCE towards the oxidation of glucose (curve 2 in Figure 7a) was investigated. The linear range of the glucose detection was from 0.001 mM to 0.577 mM ($R=0.9950$) with a slope of 875 µA cm^{-2} mM^{-1}, and a detection limit of 0.5 µM ($S/N=3$) (curve 2 in Figure 7b). It indicated clearly that Co_3O_4-rGO/GCE possessed a better catalytic activity and sensitivity towards the oxidation of glucose.

Interference is inevitable in the determination of some analytes, and thus interference of some chemicals was investigated in this work as shown in Figure 7c. Chemicals such as K^+, Na^+, Cl^- and NO^{2-} in a 20-fold did not show obvious interference to glucose detection. Organic compounds such as

AA, UA, DA, D-galactose and fructose in a same concentration have also been investigated. This result shows that only DA, D-galactose and fructose marked a poor increase of currents density, indicating the good selectivity. The stability of the sensor was also investigated. After the sensor was stored in the inverted beaker at atmosphere for 15 days, the current response to 0.5 mM glucose was decreased by 5.6% of the original current. The repeatability of the current signal of the same electrode for 0.5 mM glucose was examined in 0.1 M NaOH, and the relative standard deviation (RSD) was 4.5% for six successive measurements. The electrode to electrode repeatability was determined from the response to 0.5 mM glucose at five different sensors, and a RSD of 7.4% was achieved.
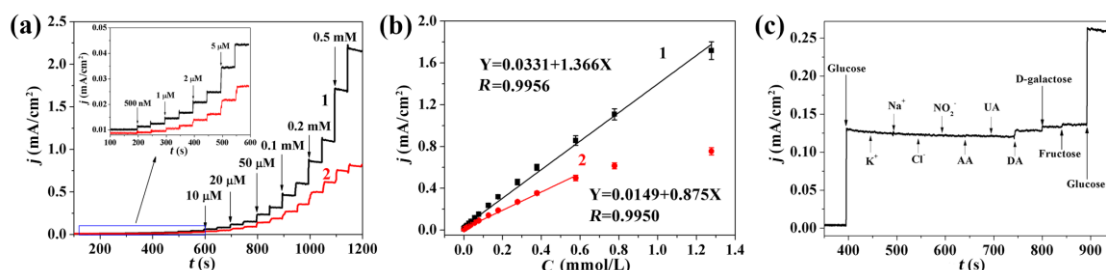

Figure 7. (a) Typical steady-state response of Co_3O_4-rGO/GCE (1) and Co_3O_4/GCE (2) to successive injection of glucose into the stirring 0.1 M NaOH. (b) The plot of the calibration curve. (c) Interference effects of some chemicals substance on glucose detection. Applied potential: 0.55 V and supporting electrolyte: 0.1 M NaOH.

The practical application of this sensor was evaluated by determination of glucose in blood serum samples. In brief, the blood samples were first diluted with 1.0 M NaOH (the final solutions were adjusted to pH=13), at which the Co_3O_4-rGO/GCE was used to monitor the glucose content. The standard colorimetric enzymatic procedure was used as a reference for checking the sensor accuracy. The results demonstrated good accuracy for the real samples. As shown in table 1, the result reveals that the practical samples have a slightly high response current density than glucose, which might be ascribed to the DA and D-galactose found in the serum sample. Thus, it could be concluded that this sensor is effective in practical applications.

Table 1. Determination of glucose in blood serum samples.

Samples	Determined by colorimetric enzymatic method (mM)	Determined by our nonenzymatic sensor (mM)	Recovery (%)	RSD (%, n=5)
1	0.0253	0.0246	102.85	3,52
2	0.127	0.122	104.10	4.37
3	0.508	0.493	103.04	3.89

Up to now, many sensors have been developed for the detection of glucose based on Co_3O_4 or rGO nanomaterials. A comparison of the performance of our newly designed sensor with those already reported in literature regarding the performance of the glucose assay was shown in Table 2 and all of

them realized glucose detection at low concentration. By comparing, it could be clearly seen that the Co_3O_4-rGO nanocomposites offered a highest sensitivity, wide linear range, faster response time and the lowest detection limit. As shown in Figure 1, the incorporation of rGO could effectively alleviate the aggregation of Co_3O_4. The evenly distributed Co_3O_4 NPs on the surface of rGO resulted in the large electrode surface area to facilitate the glucose oxidation with a high sensitivity. As shown in Figure 4, the Co_3O_4-rGO nanocomposites obtained at 150 °C for 3 h exhibited better catalytic activities, which could be ascribed to the size and dispersity of Co_3O_4 NPs. The remarkable performance of the Co_3O_4-rGO nanocomposites might be ascribed to the following. Firstly, the high conductivity of the rGO provided a highway for electron transfer and mass transfer. Secondly, the high specific surface area of the rGO could effectively alleviate the agglomeration of Co_3O_4 NPs and accordingly improve the electrochemistry performance. Finally, the Co_3O_4 NPs with size of 5-10 nm provided more electroactive sites to contact with the glucose molecules, which greatly enhanced the sensitivity of sensor.

Table 2. Comparison of various non-enzymatic glucose sensors.

Electrode	Sensitivity ($\mu A\ cm^{-2}\ mM^{-1}$)	Linear range (mM)	Detection limit (μM)	Response time (s)	Year	References
Co_3O_4-rGO	1366	0.0005-	0.18	<2	_	This work
Co_3O_4	875	0.001-0.577	0.5	<5	_	This work
Co_3O_4	36.25	0.001-2	0.97	<7	2008	[37]
CoOOH	967	0.01-0.5	10.9	<4	2012	[38]
CoO_x/rGO	79.3	0.01-0.55	2	<5	2014	[19]
Co_3O_4/graphene	_	0.05-0.3	10	_	2012	[20]
CoO/graphene	669.8	0.00083-	0.46	<3	2014	[33]
Co_2N_x/N-rGO[a]	1167	0.01-4.75	6.93	<5	2014	[39]
Co_3O_4/PbO_2	460.3	0.005-1.2	0.31	<2	2014	[15]
Cu-Co-Ni/rGO	104.68	0.01-4.3	3.05	<2	2013	[34]

[a] Nitrogen-doped reduced graphene oxide.

4. CONCLUSIONS

In summary, a highly sensitive nonenzymatic glucose sensor was developed based on the Co_3O_4-rGO nanocomposites through hydrothermal method by ethanol. The high conductivity and nanosheet structure rGO not only improved the conductivity of Co_3O_4 NPs but also provided a large specific surface area for the uniform growth of Co_3O_4 NPs, which enhanced the electron and mass transfer. A synergistic effect could be expected and accordingly a good catalytic activity toward glucose could be obtained. As a consequence, the as-prepared low-cost glucose sensor which based on the Co_3O_4-rGO nanocomposites exhibited a high sensitivity, low detection limit and good selectivity.

Overall, the current study provides a simple method to construction of nonenzymatic sensor for the rapid detection of glucose. The good response of this sensor makes it possible to be applied in real samples.

References

1. X. Wang, E. Liu and X. Zhang, *Electrochim. Acta*, 130 (2014) 253.
2. H. Huo, C. Guo, G. Li, X. Han and C. Xu, *RSC Adv.*, 4 (2014) 20459.
3. S. Badhulika, R. K. Paul, T. Terse and A. Mulchandani, *Electroanalysis*, 26 (2014) 103.
4. Y. Zhang, L. Luo, Z. Zhang, Y. Ding, S. Liu, D. Deng, H. Zhao and Y. Chen, *J. Mater. Chem. B*, 2 (2014) 529.
5. S. Alwarappan, C. Liu, A. Kumar and C.-Z. Li, *J. Phys. Chem. C*, 114 (2010) 12920.
6. X. Zhu, Q. Jiao, C. Zhang, X. Zuo, X. Xiao, Y. Liang and J. Nan, *Microchim. Acta*, 180 (2013) 477.
7. D. Zhai, B. Liu, Y. Shi, L. Pan, Y. Wang, W. Li, R. Zhang and G. Yu, ACS Nano, 7 (2013) 3540.
8. L. Yang, Y. Zhang, M. Chu, W. Deng, Y. Tan, M. Ma, X. Su, Q. Xie and S. Yao, *Biosens. Bioelectron.*, 52 (2014) 105.
9. L. Wang, J. Y. Fu, H. Q. Hou and Y. H. Song, *Int. J. Electrochem. Sc.*, 7 (2012) 12587.
10. H. Y. Yu, M. Q. Xu, S. H. Yu and G. C. Zhao, *Int. J. Electrochem. Sc.*, 8 (2013) 8050.
11. Y. Ni, L. Jin, L. Zhang and J. Hong, *J. Mater. Chem.*, 20 (2010) 6430.
12. M. Li, X. J. Bo, Z. C. Mu, Y. F. Zhang and L. P. Guo, *Sensors Actuators B Chem.*, 192 (2014) 261.
13. G. Wang, X. He, L. Wang, A. Gu, Y. Huang, B. Fang, B. Geng and X. Zhang, *Microchim. Acta*, 180 (2013) 161.
14. C. Karuppiah, S. Palanisamy, S.-M. Chen, V. Veeramani and P. Periakaruppan, *Sensors Actuators B Chem.*, 196 (2014) 450.
15. T. Chen, X. Li, C. Qiu, W. Zhu, H. Ma, S. Chen and O. Meng, *Biosens. Bioelectron.*, 53 (2014) 200.
16. L. Wang, Y. Zheng, X. Wang, S. Chen, F. Xu, L. Zuo, J. Wu, L. Sun, Z. Li, H. Hou and Y. Song, *ACS Appl. Mater. Interfaces*, (2014).
17. X. Du, I. Skachko, A. Barker and E.Y. Andrei, *Nat. Nanotechnol.*, 3 (2008) 491.
18. J. C. Meyer, A. Geim, M. Katsnelson, K. Novoselov, T. Booth and S. Roth, *Nature*, 446 (2007) 60.
19. C. Guo, X. Zhang, H. Huo, C. Xu and X. Han, *Analyst*, 138 (2013) 6727.
20. X. Wang, X. Dong, Y. Wen, C. Li, Q. Xiong and P. Chen, *Chem. Commun.*, 48 (2012) 6490.
21. W. S. Hummers Jr and R. E. Offeman, *J. Am. Chem. Soc.*, 80 (1958) 1339.
22. L. Wang, Y. Zheng, X. Lu, Z. Li, L. Sun and Y. Song, *Sensors Actuators B Chem.*, 195 (2014) 1.
23. Q. Shou, J. Cheng, L. Zhang, B.J. Nelson and X. Zhang, *J. Solid State Chem.*, 185 (2012) 191.
24. J.-M. Jung, C.-H. Jung, M.-S. Oh, I.-T. Hwang, C.-H. Jung, K. Shin, J. Hwang, S.-H. Park and J.-H. Choi, *Mater. Lett.*, 126 (2014) 151.
25. A. Gasnier, M. Laura Pedano, M. D. Rubianes and G. A. Rivas, *Sensors Actuators B Chem.*, 176 (2013) 921.
26. Y. Xu, H. Bai, G. Lu, C. Li and G. Shi, *J. Am. Chem. Soc.*, 130 (2008) 5856.
27. S. M. Choi, M. H. Seo, H. J. Kim and W. B. Kim, *Carbon*, 49 (2011) 904.

28. Z.-S. Wu, W. Ren, L. Wen, L. Gao, J. Zhao, Z. Chen, G. Zhou, F. Li and H.-M. Cheng, *ACS Nano*, 4 (2010) 3187.
29. C.-J. Yang and F.-H. Lu, *Langmuir*, 29 (2013) 16025.
30. H. Fang, Y. Pan, W. Shan, M. Guo, Z. Nie, Y. Huang and S. Yao, *Anal. Methods*, 6 (2014) 6073.
31. D. Ye, G. Liang, H. Li, J. Luo, S. Zhang, H. Chen and J. Kong, *Talanta*, 116 (2013) 223.
32. A. J. Bard and L. R. Faulkner, *Electrochemical Methods: Fundamentals and Applications*, John Wiley and Sons, Inc., New York (2001) pp. 156.
33. S. Ci, S. Mao, T. Huang, Z. Wen, D.A. Steeber and J. Chen, *Electroanalysis*, 26 (2014) 1.
34. H. Liu, X. Lu, D. Xiao, M. Zhou, D. Xu, L. Sun and Y. Song, *Anal. Methods*, 5 (2013) 6360.
35. A. J. Bard and L. R. Faulkner, *Electrochemical Methods: Fundamentals and Applications*, John Wiley and Sons, Inc., New York (2001) pp. 471.
36. M. Jafarian, F. Forouzandeh, I. Danaee, F. Gobal and M. G. Mahjani, *J. Solid State Electrochem.*, 13 (2009) 1171.
37. Y. Ding, Y. Wang, L. Su, M. Bellagamba, H. Zhang and Y. Lei, *Biosens. Bioelectron.*, 26 (2010) 542.
38. K. K. Lee, P. Y. Loh, C. H. Sow and W. S. Chin, *Electrochem. Commun.*, 20 (2012) 128.
39. L. Kong, Z. Ren, S. Du, J. Wu and H. Fu, *Chem. Commun.*, 50 (2014) 4921.